

Z-Group Ketone Chain Transfer Agents for RAFT Polymer Nanoparticle Modification via Hydrazone Conjugation

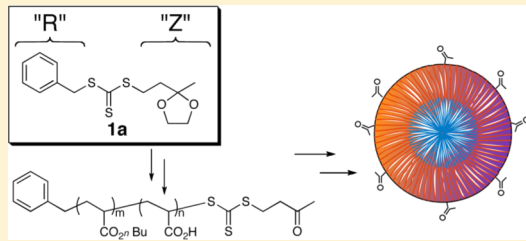
Saibal Bandyopadhyay,[†] Xin Xia,[†] Andrei Maiseiyeu,[‡] Georgeta Mihai,[‡] Sanjay Rajagopalan,[‡] and Dennis Bong*,[†]

[†]Department of Chemistry, 100 W. 18th Avenue, The Ohio State University, Columbus, Ohio 43210, United States

[‡]The Davis Heart and Lung Institute, 473 W. 12th Avenue, The Ohio State University, Columbus, Ohio 43210, United States

Supporting Information

ABSTRACT: A ketal-containing trithiocarbonyl compound has been synthesized and characterized as a chain transfer agent (CTA) in reversible addition–fragmentation transfer (RAFT) polymerization. The ketal functionality does not interfere with RAFT polymerization of acrylate monomers, which proceeds as previously reported to yield macro-CTA polymers and block copolymers. Postpolymerization ketal cleavage revealed ketone functionality at the polar terminus of an amphiphilic block copolymer. Hydrazone formation was facile in both organic solution and aqueous buffer where polymer nanoparticle assemblies were formed, indicating a conjugation/end-functionalization yield of 40–50%. Conjugation was verified with fluorescein, biotin, and Gd-DOTA derivatives, and though the trithiocarbonate linkage is hydrolytically labile, we observed stable conjugation for several days at pH 7.4. and 37 °C. As expected, streptavidin binding to biotinylated polymer micelles was observed, and size-change-based relaxivity increases were observed when Gd-DOTA hydrazide was conjugated to polymer micelles. Cell uptake of fluorescently labeled polymer micelles was also readily tracked by FACS and fluorescence microscopy. These polymer derivatives demonstrate a range of potential theranostic/biotechnological applications for this conveniently accessible keto-CTA, which include ligand-based nanoparticle targeting and fluorescent/MR nanoparticle contrast agents.



Accessible strategies for controlled radical polymerization such as RAFT¹ and ATRP² have enabled a dramatic expansion in the number of applications for which synthetic polymers may play a role. The chain transfer agent (CTA) in RAFT polymerization facilitates block copolymer synthesis, controls polydispersity, and presents an opportunity for polymer end-functionalization. Functionality pendant to the CTA will be presented at a polymer terminus once polymerization has been halted. This aspect of controlled radical polymerization has been previously exploited to end-functionalize polymers and, by extension, surface-functionalize polymer assemblies.^{1c,2b,3} End-functionalization strategies of linear polymers have minor impact on packing interactions along the polymer strand⁴ relative to random side-chain functionalization and are thus less likely to affect polymer assembly. By choosing the order of monomer use in an amphiphilic copolymer RAFT synthesis, one may determine the functionality at each termini. Thus, modification at the terminus of the polar block should result in presentation of that functionality on the surface of an aqueous-phase assembly, while the same functionality would be buried when assembly occurs in nonpolar media.⁵

Surface derivatization of polymer assemblies such as micelles is often desirable for biomedical applications, in order to promote biomolecular interactions or to block them.³ Installation of poly(ethylene glycol) (PEG) on the surface of nanoparticles and liposomes⁶ is well-known to reduce binding

of serum proteins, opsonization, and immunoclearance.⁷ These surface protected assemblies have been shown to have longer in vivo circulation times and altered tissue deposition relative to their undecorated counterparts.⁸ The use of appropriately functionalized CTAs has thus been used to synthesize polymer micelles that surface-display poly(ethylene oxide) (PEO) in order to take advantage of the immuno-evasive properties imparted by surface presentation of a hydrophilic polymer.⁵ Biotin-derivatized RAFT CTAs⁹ or ATRP initiators¹⁰ have been used to enable protein conjugation to polymer scaffolds. There have also been numerous reports of incorporation of thiol groups as polymer-end nucleophiles to couple with electrophilic disulfides or halides for postassembly functionalization or transformation of the thiol into other functionalities.^{1a,11} This is especially facile with RAFT polymers terminated with a trithiocarbonate moiety that may be easily transformed into a thiol-terminated polymer. Thus, through the use of derivatized RAFT agents, carboxy, amino, thiol, azide, and more complex metal ligands, fluorescent and biomolecular tags have been incorporated selectively at the terminus of a RAFT polymer.^{1a,12} While thiol chemistry provides a generally useful platform for further polymer modification, the thiol itself is prone to oxidation under ambient conditions; further, addi-

Received: July 23, 2012

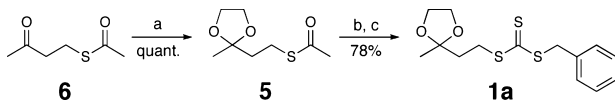
Revised: August 22, 2012

tional chemoselective functionality would broaden the utility of this method. With this in mind, we designed and synthesized a Z-group acetal-derivatized trithiocarbonate chain transfer RAFT agent that would yield a ketone-terminated RAFT polymer.

Ketone reaction with hydrazine and aminoxyethers to form hydrazone and oxime linkages has considerable precedent as a bioconjugation strategy.¹³ Like disulfides, these stabilized imines are exchange-active covalent bonds that are hydrolytically labile under acidic conditions, whereas disulfides are labile under reducing conditions. This property has been previously exploited to produce hydrazone/oxime linked carrier systems¹⁴ are stable at normal physiological pH but will release cargo once acidic pH is encountered, such as within an endosomal compartment or the slightly acidic solid tumor microenvironment. Hydrazone/oxime formation may be carried out in either organic or aqueous conditions and is remarkably chemoselective, with no alternative reaction outcomes observed with either the amine or keto components under normal physiological conditions. Thus, polymer termination with keto functionality may be derivatized by any synthetic hydrazine or aminoxyether containing molecule, in aqueous or organic milieu, with minimal concern for polymer self-reaction (as with thiol oxidation). Though postpolymerization ketone modification requires additional handling, prior installation of hydrophilic groups on the CTA may lead to poor chain extension with hydrophobic monomers due to solubility issues.^{5,15} Recently, Maynard¹⁶ and Fulton¹⁷ have demonstrated the polymer end-incorporation of aminoxyether and aldehyde groups, using RAFT chain transfer agents derivatized at the reinitiator site. These methods both utilized S-alkyl-S'-(α,α -dimethyl- α'' -acetic acid)trithiocarbonate¹⁸ chain transfer agents with aminoxyether or aldehyde containing groups amidated to the dimethyl acetic acid moiety, which serves as the “R” group reinitiator on the RAFT CTA. We report herein a complementary synthetic approach that places a keto group on the “Z” group of the CTA, which does not dissociate from the trithiocarbonate during radical polymerization.

There are many appealing aspects of placing the chemoselective “handle” on the reinitiating “R” group: the handle is connected to the polymer via a hydrolytically stable carbon–carbon bond, and the “Z” group may then be converted to the chemically versatile thiol group or easily removed.^{1a,11a} Preparation of the dimethylacetic acid CTAs does require multistep synthesis, albeit straightforward, with a range of yields from high to low.¹⁸ We demonstrate herein that the “Z” group functionalization remains chemically stable on polymer assemblies over days at physiologically relevant conditions of pH 7.4 and 37 °C, suggesting that the trithiocarbonate linkage is sufficiently stable to be useful in bioapplications. Our approach to the Z-keto CTA is a flexible, high yielding approach (Scheme 1) that permits variation in the R group,^{1a,d} which may be convenient or necessary for some monomers.

Scheme 1. Synthesis of 1a^a



^aReagents and conditions: (a) D-tartrate, ethylene glycol, Dean–Stark THF reflux; (b) NaOH_(aq); (c) CS₂, benzyl bromide.

Z-group end-functionalization further avoids competitive reinitiation by AIBN-derived radicals.¹⁹ We demonstrate the utility of this approach by surface-labeling keto polymer assemblies with hydrazides bearing fluorophores, MRI contrast agents, and biotin. As expected, we observe fluorescence anisotropy, relaxivity increases, and streptavidin binding consistent with modification of the polymer assemblies. Furthermore, polymer nanoparticle uptake in A549 and MCF-7 cell lines was tracked with an end-labeled fluorescent polymer. Thus, this range of conjugation chemistry demonstrates how this keto-RAFT agent could be applied in a wide range of targeting and theranostic applications.^{8a}

EXPERIMENTAL SECTION

General. All commercially available materials were purchased from Sigma-Aldrich. GdDOTA hydrazide was synthesized following literature procedures.^{14a} Monomers were purified using an alumina column to remove inhibitor and stored at −20 °C. AIBN was recrystallized from methanol. All polymerization solvents were degassed prior to use under a nitrogen atmosphere. Concentration of 1a and ratio of 1a:AIBN was held constant in all polymerizations. Theoretical molecular weight ($M_{w,t}$) was calculated according to $M_{w,t} = (nBA_{mw}[nBA]C)/[1a]$ where nBA_{mw} is the molecular weight of repeat unit and C is conversion. NMR and mass spectra were acquired on a 400 MHz Bruker Avance instrument and a Bruker MicroTOF ESI, respectively. Fluorescence anisotropy measurements were acquired at 25 °C on a PerkinElmer LS-50B fitted with polarizers. Transmission electron microscopy samples were prepared on 200 mesh Formvar-carbon film copper grids, stained with uranyl acetate and analyzed on a FEI Tecnai G2 Bio TWIN TEM.

Relaxivity Measurements. Relaxivities (r_1 longitudinal) were determined as the slope of the curve obtained by plotting inverse relaxation ($1/T_1$) against the range of gadolinium concentration. Measurements were conducted using a 1.5 T scanner at 25 °C (Magnetom, Avanto MRI scanner, Siemens Medical Solutions, Erlangen, Germany). Samples (100 μ L) were prepared based on Gd concentrations (2–0.03 mM) and analyzed in a sealed polypropylene 96-well plate in a styrene box filled with water. Relaxation curves for T_1 were obtained by 2D imaging with an inversion–recovery turbo spin-echo (IRTSE) pulse sequence. The following inversion times were applied: 30, 60, 90, 120, 150, 250, 400, 600, 800, 1200, 1600, and 2000 ms. Relaxation times (r_1) were calculated from each slope of the linear relation between $1/T_1$ and Gd concentration. Gadolinium concentration was determined by inductively coupled plasma optical emission spectroscopy (ICP-OES).

Cell Uptake. Human breast adenocarcinoma (MCF-7) and human lung carcinoma (A549) cell lines were maintained in GIBCO Dulbecco's Modified Eagle Medium: Nutrient Mixture F-12 (DMEM/F-12) media with 10% FBS and 1% penicillin–streptomycin. All FACS samples were run on a LSR-II flow cytometry instrument using FITC-A and PE-A lasers, and the results were analyzed using FlowJo software. Cell microscopy images were acquired on an Zeiss Axio Observer A1.

Synthesis of Benzyl 2-(2-Methyl-1,3-dioxolan-2-yl)-ethyltrithiocarbonate (1a). S-Acetyl-4-mercaptop-2-butanone (1.46 g, 0.01 mol) is commercially available but was readily prepared from Michael addition of CH₃COSK to methyl vinyl ketone²⁰ and converted to the acetal by reaction with ethylene glycol (2.48 g, 0.04 mol) and D-tartrate (0.05 g) in refluxing THF for 12 h using a Dean–Stark apparatus. The reaction mixture was concentrated under reduced pressure, dissolved in 80 mL of CH₂Cl₂, washed with saturated aqueous NaHCO₃, dried over anhydrous Na₂SO₄, and concentrated under reduced pressure to give the desired acetal²¹ in quantitative yield. The thiol ester (0.5 g, 2.63 mmol) was hydrolyzed under nitrogen in 1:1 methanol/0.2 M NaOH solution (30 min), then treated with sodium bicarbonate (0.22 g, 2.6 mmol), CS₂ (0.27 mL, 4.5 mmol), and benzyl bromide (0.53 mL, 4.5 mmol), and then stirred overnight. The reaction mixture was purified by silica gel

chromatography (15% EtOAc/hexanes) following aqueous work-up ($\text{CH}_2\text{Cl}_2/\text{H}_2\text{O}$) to give pure **1a** as a yellow liquid in 78% overall yield. ^1H NMR (CDCl_3) δ : 7.26 (5H, m), 4.55 (2H, s), 3.90 (4H, m), 3.39 (2H, m), 2.01 (2H, m), 1.31 (3H, s). ^{13}C NMR (CDCl_3) δ : 223.9, 135.3, 129.4, 128.8, 127.9, 109.1, 65.0, 41.5, 37.3, 31.8, 24.2. HRMS (ESI): m/z calcd for $\text{C}_{14}\text{H}_{18}\text{O}_2\text{S}_3\text{Na} [\text{M} + \text{Na}]^+$ 337.0366. Found 337.0404.

Benzyl-3-oxobutyltrithiocarbonate (1b). **1a** (0.04 g) was stirred in methanol with 0.5% TFA at room temperature for 1 h. Solvent was removed, and reaction mixture was redissolved in dichloromethane and washed with $\text{NaHCO}_3(\text{sat})$. After concentration **1b** was obtained as yellow oil in quantitative yield. ^1H NMR (CDCl_3) δ : 7.34 (5H, m), 4.62 (2H, s), 3.59 (2H, t, $J_{\text{HH}} = 6.4$ Hz), 2.93 (2H, t, $J_{\text{HH}} = 6.4$ Hz), 2.18 (3H, s). ^{13}C NMR (CDCl_3) δ : 223.8, 206.2, 135.3, 129.5, 128.9, 128.0, 42.3, 41.7, 30.4, 30.1. HRMS (ESI): m/z calcd for $\text{C}_{12}\text{H}_{14}\text{OS}_3\text{Na} [\text{M} + \text{Na}]^+$ 293.0104. Found 292.9182.

Hydrazone Formation (Small Molecule). Ketone **1b** (0.010 g, 0.037 mmol) was dissolved in methanol with biotin hydrazide **3** (0.010 g, 0.047 mmol) followed by a catalytic amount (5 μL) of acetic acid. The resulting reaction mixture was stirred at room temperature for 1 h and concentrated under reduced pressure to give pale yellow solid which was dissolved in $d_6\text{-DMSO}$ and analyzed by ^1H NMR. HRMS (ESI): m/z calcd for $\text{C}_{22}\text{H}_{30}\text{N}_4\text{NaO}_2\text{S}_4 [\text{M} + \text{Na}]^+$ 533.1149. Found 533.1145.

General Procedure for Polymer–Hydrazone Conjugation. PnBA-*b*-PAA ($\text{Pb}_{(m,n)}$, 0.012 mmol) was dissolved in 10 mL of methanol and CH_2Cl_2 (3:1) mixture followed by the addition of hydrazide (or semithiocarbazide) derivative (0.011 mmol) and 10 μL of TFA. The resulting reaction mixture was stirred for 8 h, then concentrated under reduced pressure, and dried under high vacuum to yield a solid product that could be redissolved in dry methanol.

Polymerization Kinetics. *n*-Butyl acrylate (2.92 g, 22.8 mmol) and **1a** (0.03 g, 0.095 mmol) were dissolved in 3 mL of DMF and heated to 70 °C in a sand bath under nitrogen, with DMSO (1.0 mL) added as an internal standard. Polymerization was initiated with the addition of AIBN (1.57 mg, 0.0095 mmol). Reaction aliquots were collected every 10 min and quenched by cooling in dry ice acetone bath under ambient atmosphere. Time point samples were analyzed using the combination of ^1H NMR spectroscopy and gel permeation chromatography (GPC/SEC).

General Polymerization Procedure ($\text{Pa}_{(30,0)}$). As above, CTA **1a** (0.12 g, 0.38 mmol) and monomer *n*-butyl acrylate (2.92 g, 22.8 mmol) were dissolved in 25 mL of DMF with a DMSO (1.06 g) internal standard and heated to 70 °C. Polymerization was initiated by addition of AIBN (6.0 mg, 0.038 mmol) and quenched after 53% conversion. Unreacted monomer and solvent were removed under reduced pressure to obtain the macro-CTA, PnBA, as an oily liquid that was analyzed by GPC to obtain the following parameters: $M_n(\text{GPC}) = 4210$, $M_w/M_n = 1.19$ (theoretical molecular weight $M_{w,t} = 4390$).

General Procedure for Block Copolymer Synthesis ($\text{Pa}_{(30,28)}$). In a 50 mL round-bottom flask *tert*-butyl acrylate (2.92 g, 22.8 mmol) and macro-CTA ($\text{Pa}_{(30,0)}$, 1.0 g, 0.153 mmol) were dissolved in 23 mL of DMF and heated to 70 °C after thorough degassing. After stirring for 5 min, polymerization was initiated with the addition of AIBN (0.006 g). Reaction was followed by ^1H NMR spectroscopy and was quenched after 53% monomer was consumed. Theoretical molecular weight = 8455, $M_n(\text{GPC}) = 7797$, $M_w/M_n = 1.21$.

General Procedure for Polymer Acidolysis ($\text{Pb}_{(m,n)}$). Block copolymer ($\text{Pa}_{(m,n)}$) was dissolved in 2 mL of methylene chloride with 8 mL of TFA and stirred for 3 h. Volatiles were removed under reduced pressure, and the resulting solid was dissolved in CH_2Cl_2 and washed with 1 N HCl to the organic layer concentrated to yield $\text{Pb}_{(m,n)}$; the block copolymer as a pale yellow solid.

General Procedure for Polymer Nanoparticle Formation. A methanolic solution of $\text{Pb}_{(m,n)}$ block copolymer (0.002 g) was placed in a test tube and methanol was removed under nitrogen stream to form polymer film which were subsequently dried under vacuum. Polymer films were hydrated with 1 mL of DPBS buffer and sonicated for 2 min using a benchtop sonicator.

Purification of Hydrazone–Nanoparticle Suspensions. Crude conjugation reaction mixtures in methanol (0.002 g) were dried to polymer films as described above then hydrated with 1 mL of DPBS buffer and sonicated to produce polymer nanoparticles, and pH adjusted to 7.6 with NaHCO_3 saturated solution as necessary. Polymer nanoparticle suspensions were washed with DPBS (1 mL/10 min) in a centrifuge size exclusion filter appropriate for the polymer length (e.g., 10 and 30 kDa exclusion for conjugates with 6 kDa $\text{Pa}_{(30,28)}$ and 19.5 kDa $\text{Pa}_{(100,89)}$, respectively). Centrifuge filtration was performed at 4000 rpm for 2 h.

RESULTS AND DISCUSSION

The following studies focus on validation of the acetal-derivatized trithiocarbonate as an effective chain transfer agent for RAFT polymerization and quantification of accessible ketone-terminated polymer. The general polymer architecture is an amphiphilic block copolymer of *n*-butyl acrylate and acrylic acid, PnBA-*b*-PAA, with free ketone terminating the PAA block. Similar amphiphilic copolymers with poly(acrylic acid) have been found to form “kinetically” frozen micelles of \sim 200 monomer length;²² we have synthesized polymers with \sim 50 mol % acrylic acid with total length of \sim 200, 100, and 60 monomers, which we term $\text{Pb}_{(100,89)}$, $\text{Pb}_{(49,48)}$, and $\text{Pb}_{(30,28)}$, respectively (Figure 1 and Table 1). We further demonstrate polymer–hydrazide conjugation and nanoparticle display of a fluorescent tag, protein-targeting ligand, and MRI-contrast agent.

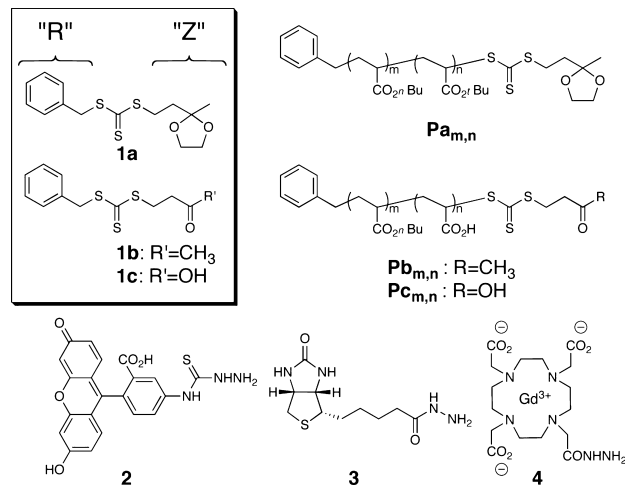


Figure 1. (top left) Chain transfer agents used with reinitiator “R” and “Z” groups indicated. General polymer architectures and hydrazine derivatives used in polymer and CTA conjugation are shown.

Synthesis and Conjugation of Keto Chain Transfer Agent. There have been numerous reports of polymer end-functionalization that utilize trithiocarbonate RAFT agents that are modified at the reinitiator site. Much of this exploration was enabled by convenient synthesis of S-alkyl-S’-(α,α -dimethyl- α' -acetic acid) trithiocarbonates,¹⁸ which are then used to acylate an appropriately derivatized amine or alcohol. There have been far fewer reports on modification of the “Z” group on trithiocarbonate RAFT agents, possibly due to perceived lability of the trithiocarbonate to nucleophilic cleavage. Detailed studies on nucleophilic cleavage of dithiocarbonate RAFT agents indicated strong dependence of cleavage rates on conditions.²³ The synthesis of ketone-derivatized CTAs is straightforward and high-yielding (Scheme 1).

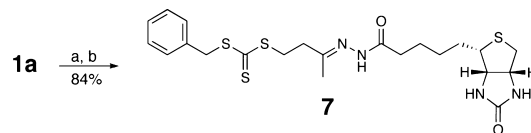
Table 1. Macro-CTA and Block Copolymer Properties

polymer	M_n (kDa) ^a	M_w/M_n	DP ^b	ketone (%) ^c
Pa_(30,0)	4.2	1.19	30	n.d.
Pa_(30,28)	7.8	1.21	58	n.d.
Pb_(30,28)	6.1*	n.d.	58	52, 61
Pa_(49,0)	6.7	1.22	49	n.d.
Pa_(49,48)	12.8	1.24	97	n.d.
Pb_(49,48)	10.0*	n.d.	97	41, 45
Pa_(100,0)	13.1	1.16	100	n.d.
Pa_(100,89)	24.6	1.23	189	n.d.
Pb_(100,89)	19.5*	n.d.	189	46, 53

^a M_n and M_w/M_n determined by GPC, except for asterisks, which indicate theoretical molecular weight. ^bDegree of polymerization, calculated using M_n . ^cKetone accessible in polymer determined by FTSC conjugation. n.d. = not determined.

The acetal transfer agent **1a** was used in all polymerizations and deprotected under acidic conditions to yield the ketone-terminated polymer product. It is well-known that nucleophiles such as primary amines and hydrazine may cleave the trithiocarbonate, which reasonably raises concerns that the keto end group may be cleaved from the polymer terminus in the process of conjugation with acylhydrazides. While the trithiocarbonate clearly survives acylation conditions with amine nucleophiles, hydrazides are more reactive as nucleophiles. The conjugation reaction was performed on the soluble keto RAFT agent itself with biotin–hydrazide under acidic conditions, which are known to be favorable for hydrazone formation and suppress²³ the hydrazidolysis of the trithiocarbonate.

Biotin–hydrazide Reaction with CTA. Gratifyingly, *in situ* ¹H NMR monitoring of the conjugation of **1b** with **3** in *d*₄-methanol indicated clear formation of the hydrazone in 84% yield with the remaining material unreacted ketone (Figure 2). Conversion was measured by the relative integration of ketone and hydrazone methyl resonances, which appear as a singlet in the ketone (2.18 ppm) and a pair of singlets in the hydrazone due to syn- and anti-hydrazone configurations (1.85, 1.82 ppm). Similar conditions were used for postpolymerization hydrazone conjugation.

Scheme 2. Hydrazone Conjugation^a

^aReagents and conditions: (a) 1% TFA in methanol; (b) 1% acetic acid in methanol and **3**.

RAFT Polymerization. It was first established that the acetal chain transfer agent **1a** was an effective RAFT agent. Indeed, the kinetic signatures of reversible chain transfer²⁴ were observed in the linear growth of $\ln(M_0/M_t)$ over time (Figure 3) for *n*-butyl acrylate monomer (*M*) when a ratio of CTA:*n*-BA 1:239 was used. Furthermore, polymer M_n (GPC) dependence on monomer conversion (¹H NMR) indicated the linear trend with good fit to theoretical M_n while polydispersity (PDI) remained relatively flat and ~1.2 PDI, as judged by GPC analysis. Thus, polymer growth exhibits pseudo-first-order kinetics and low PDI, consistent with chain transfer characteristics of known RAFT agents. Overall, narrow polydispersity throughout the polymerization suggests effective chain transfer even at high monomer conversion (>70%). We employed CTA **1a** in the preparation of 1:1 block copolymers of *tert*-butyl acrylate and *n*-butyl acrylate, which on acidolysis yielded PnBA-*b*-PAA-keto. Block copolymers were prepared with total monomer units of ~58, 97, and 189 that exhibited PDIs of ~1.2 (Table 1).

Quantification of Accessible Polymer-Displayed Ketone. Each of these block copolymer products could be functionalized with acyl hydrazides with 40–60% yield relative to total polymer. Functional incorporation of the keto group for all polymer lengths was conveniently quantified by conjugation with fluorescein-5-thiosemicarbazide (FTSC). Conjugation was conveniently carried out in methanol with catalytic acetic acid, where the polymers are soluble, and could also be carried out in aqueous buffer at pH 7, where PnBA-*b*-PAA-keto polymers are assembled into low-polydispersity nanoparticles with diameters of 24, 38, and 78 nm, correlating with increasing polymer length (Figure 5). Negative-stain TEM indicated the presence of clusters of uniform spherical particles (Figure 5, Supporting

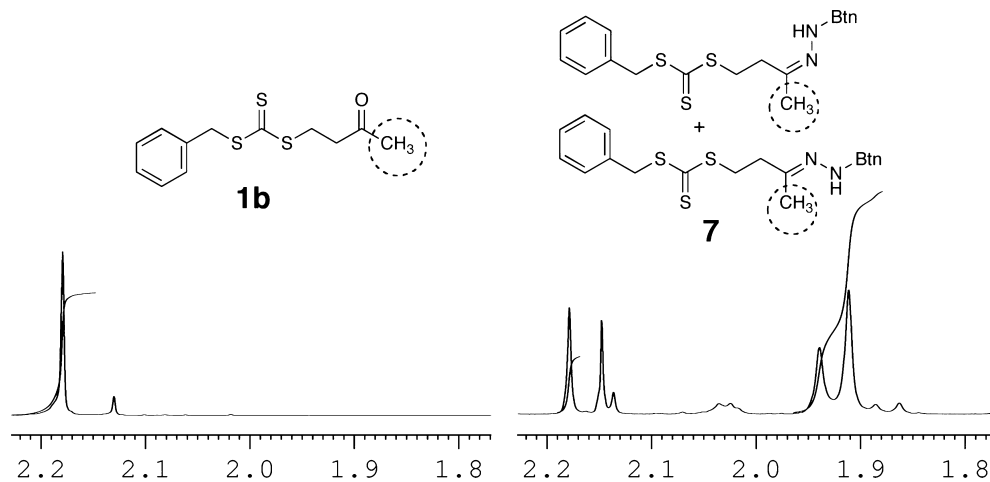


Figure 2. ¹H NMR of **1b** (left) and hydrazone **7** (right). Hydrazone methyl peaks shift upfield as two singlets representing syn and anti stereoisomers relative to the ketone methyl singlet of **1b**. The singlet at 2.15 ppm is acetic acid while the smaller singlet at 2.13 ppm in both spectra is a nonreactive impurity.

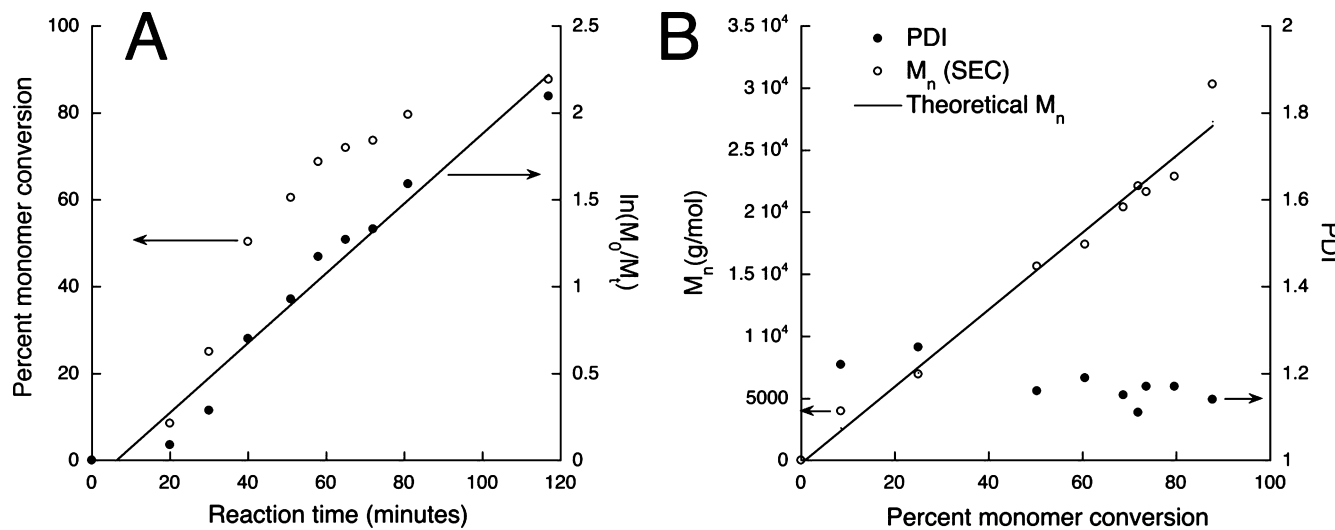


Figure 3. Kinetic plots of *n*-butyl acrylate (nBA) polymerization in the presence of **1a** indicating (A) steady state conditions and (B) consistently low PDI as a function of monomer conversion with good correlation between experimental and theoretical M_n ($M_{w,t}$). Monomer:**1a**:AIBN stoichiometry was 239:1:0.1.

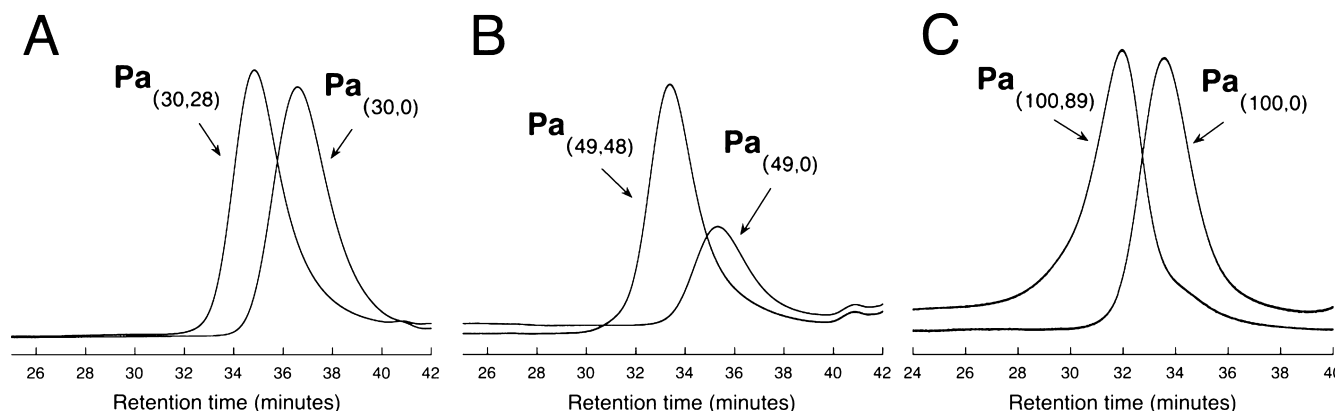


Figure 4. Chain extension studies on macroCTAs to produce block copolymers: (A) $\text{Pa}_{(30,0)}$ to $\text{Pa}_{(30,28)}$; (B) $\text{Pa}_{(49,0)}$ to $\text{Pa}_{(49,48)}$; (C) $\text{Pa}_{(100,0)}$ to $\text{Pa}_{(100,89)}$. Generation of macro-CTAs as intermediates in copolymer synthesis was confirmed by chain extension studies in these three size regimes.

Information). The FTSC-conjugated polymer was concentrated into a film from methanol, hydrated in DPBS buffer to yield polymer nanoparticles, and then washed with buffer using a Centricon filter to remove unreacted FTSC. Particle size was not detectably changed relative to the free ketone particles upon hydrazone formation, as judged by DLS. Analysis of the unreacted FTSC in the filtrate indicated ~50% retention by the nanoparticle suspension. In contrast, reaction of the fluorescein semithiocarbazine with a control polymer in which the CTA bears a carboxylic acid in place of a ketone led to complete loss of fluorescein absorbance from the nanoparticle suspension upon filtration. Conjugated FTSC was rapidly cleaved from the nanoparticles by hydrazinolysis at pH 9.5 and quantified by measurement of fluorescein UV absorbance, which confirmed the ~50% yield for block copolymers of 6, 10, and 19.5 kDa molecular weight (Table 1). Though the FTSC linkage is not stable to strongly basic treatment with hydrazine, labeled nanoparticles exhibit less than 1% loss in fluorescence after 2 days incubation at pH 7.4, DPBS at 37 °C, indicating that the conjugation is sufficiently stable in biologically relevant conditions. Nanoparticle-FTSC coupling was also tracked by monitoring fluorescence anisotropy change. As expected, anisotropy increased significantly in the keto nanoparticle

reaction, while in the control nanoparticle reaction anisotropy change was weaker (Figure 5). Though an anisotropy increase was observed with the carboxylate-terminated nanoparticle control, this likely represents minor nonspecific binding given the relatively low fluorescence intensity of the sample.

Polymer Nanoparticle Biotinylation. Particle functionalization with protein ligands enables targeting to specific biological targets directly or through antibody conjugation. We demonstrate this functionality with biotin modification of the polymer nanoparticle surface. Hydrazide conjugation of biotin hydrazide with ketone-terminated polymer was performed in a similar fashion to FTSC coupling. Biotin binding was also assessed by fluorescence anisotropy change using streptavidin-FITC. Indeed, treatment of fluorescently labeled streptavidin with surface biotinylated polymer nanoparticles resulted in the expected increase in FITC anisotropy, consistent with the larger size of the putative nanoparticle-bound streptavidin fluorophore relative to the protein. Incubation of streptavidin-FITC with non-biotinylated polymer nanoparticles did not significantly alter fluorescence anisotropy, nor did incubation with free biotin (Figure 5); this is also expected given the minor change in protein size upon small-molecule binding. Biotin titration of streptavidin-FITC is accompanied

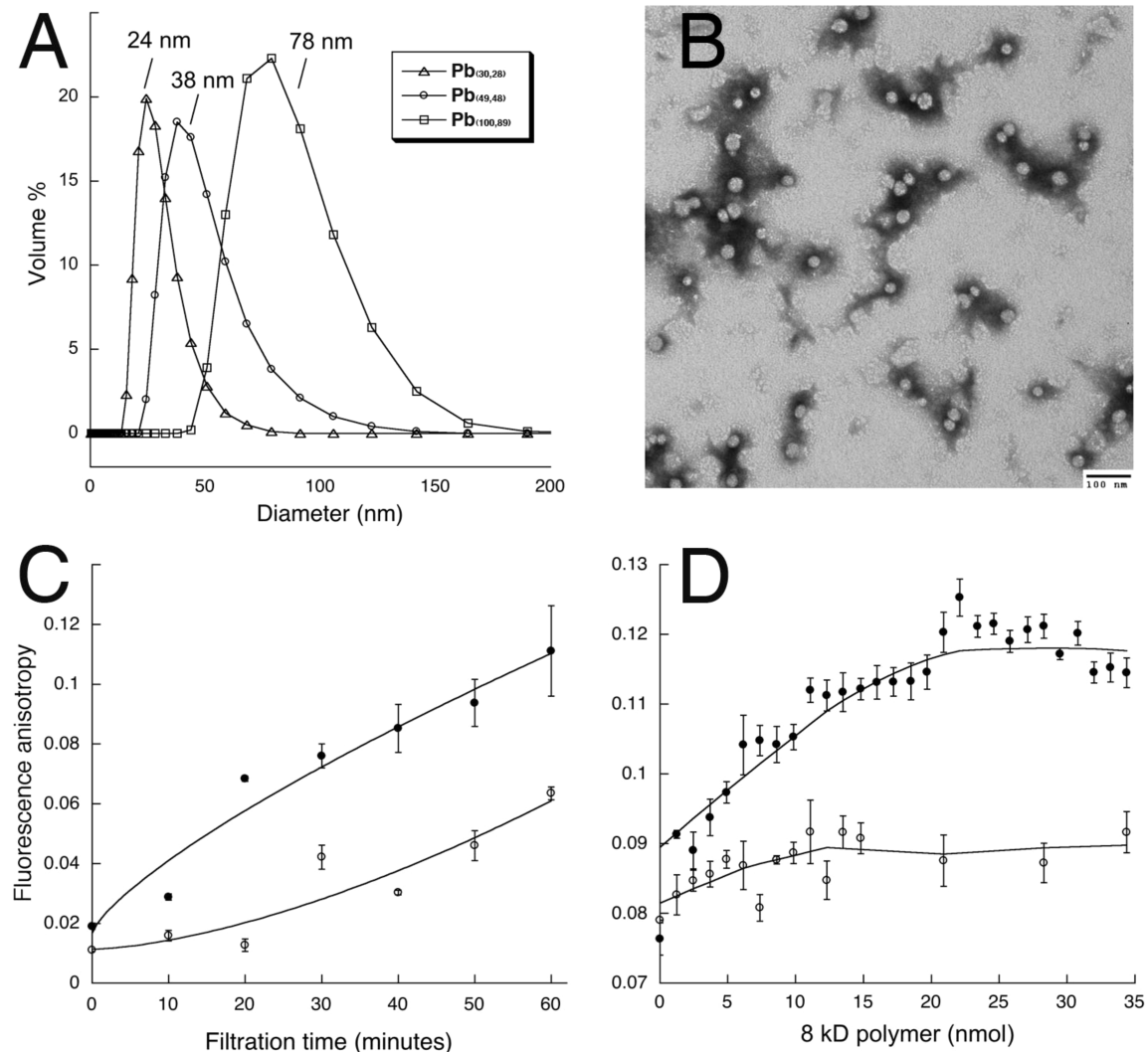


Figure 5. (A) Dynamic light scattering measurements (DPBS, pH 7.4) of polymer nanoparticles indicated. (B) Negative stain transmission electron micrographs of $\text{Pb}_{(49,48)}$, with 100 nm scale bar shown. Fluorescence anisotropy measurements of ketone polymer $\text{Pb}_{(100,89)}$ (●) and control polymer $\text{Pc}_{(100,89)}$ (○) during (C) nanoparticle conjugation with FTSC 2 and (D) incubation streptavidin–FITC following conjugation with biotin–hydrazide 3.

by an increase in fluorescence intensity. Though this increase in emission on biotin binding is not well-understood, it provides an analytical measure of concentration.²⁵ By this empirical method, a much higher concentration of polymer-displayed biotin is required to attain the same increase in streptavidin–FITC emission relative to free biotin (Supporting Information). The origin of this difference is unclear and may indicate diminished accessibility²⁶ of the biotinylated polymer terminus or an altered FITC emission environment for the protein–nanoparticle complex relative to the protein–biotin complex.

Conjugation of MRI Contrast Agent to Ketone Nanoparticles. Nanoparticle accumulation in solid tumors and atherosclerotic plaques²⁷ through the enhanced permeation and retention (EPR) effect has generated considerable interest in their use as delivery and imaging agents. Significant advantages in tumor/plaque imaging are presented by nanoparticle conjugation to traditional magnetic resonance imaging (MRI) contrast agents such as gadolinium complexes: increased retention in the tissue of interest and enhanced MRI sensitivity. The gadolinium DOTA hydrazide complex 4 was incubated with the keto-nanoparticle ($\text{Pb}_{(100,89)}$) suspension as well as the

carboxylate nanoparticle control ($\text{Pc}_{(100,89)}$) and purified by dialysis. Conjugation of 4 to nanoparticle $\text{Pb}_{(100,89)}$ significantly increased Gd relaxivity. Over the pH range 4–8 and field strength of 1.5 T (60 MHz), conjugate relaxivity per Gd^{3+} was $\sim 50 \text{ mM}^{-1} \text{ s}^{-1}$, about 17 times higher than commercial Gd(DOTA) ($3.0 \text{ mM}^{-1} \text{ s}^{-1}$). Such an increase in relaxivity could derive from more limited motion of the Gd complex when bound to the polymer assembly. Protein, polymer, and particle-bound gadolinium complexes have been previously reported to have increased Gd relaxivities²⁸ with r_1 values as high as $15.9 \text{ mM}^{-1} \text{ s}^{-1}$ for polymer-caged nanoparticles²⁹ and $41 \text{ mM}^{-1} \text{ s}^{-1}$ for Gd-bound high-density lipoprotein.³⁰ Similarly, our study shows that Gd(DOTA)–hydrazone conjugation to polymer nanoparticles from $\text{Pb}_{(100,89)}$ elicits a dramatic increase in r_1 relaxivity per Gd ion. Contrast agents possessing hypersensitivity warrant further detailed investigation, especially for in vivo imaging applications where high sensitivity is critical. No gadolinium was detectable in the control nanoparticle sample ($\text{Pc}_{(100,89)}$) following dialysis. Notably, similar relaxivity over a wide pH range of our nanoparticle contrast agent (Figure 6) suggests utility in acidic

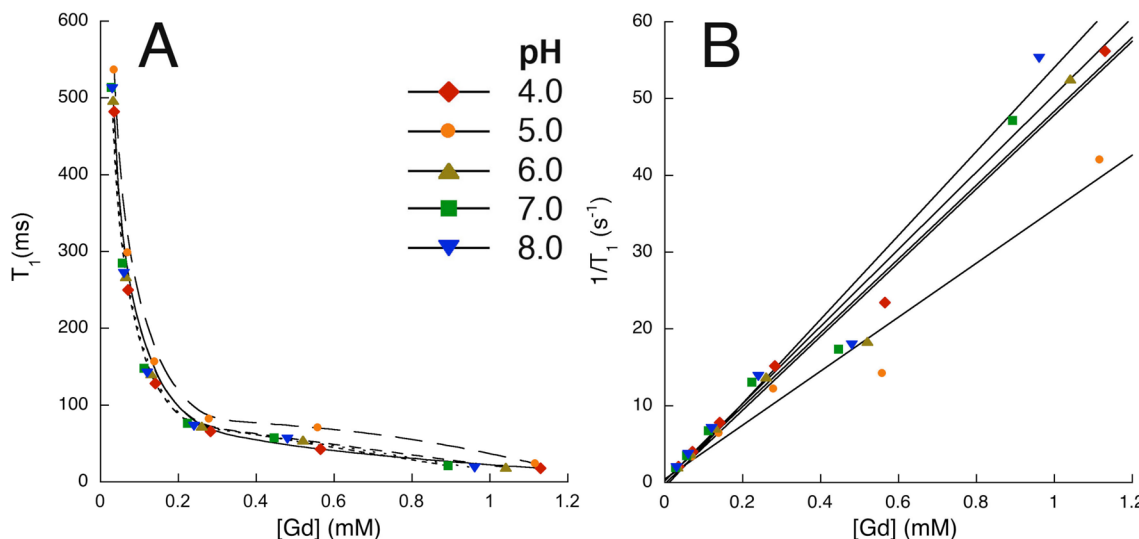


Figure 6. Dependence of gadolinium (A) T_1 and (B) $1/T_1$ on concentration of Gd-DOTA hydrazide 4 incubated with nanoparticles from keto polymer $\mathbf{Pb}_{(100,89)}$ following dialysis purification. Relaxivities over the pH range 4–8 are 48.1, 35.2, 48.0, 50.2, and $54.7 \text{ mM}^{-1} \text{ s}^{-1}$, respectively (see legend).

microenvironments as well as trithiocarbonate stability in basic aqueous conditions. It is possible that decreased accessibility to the trithiocarbonate linkage via polyacrylate neutralization affords greater hydrazone stability in acidic pH regimes.

Tracking Cellular Uptake of Fluorescent Nanoparticles. To showcase the potential utility of the keto-CTA to track polymer biodistribution, we studied the cell uptake of fluorescently labeled nanoparticles. Mixed films of fluorescently labeled keto PnBA-*b*-PAA (19.5 kDa) and carboxylate terminated polymer of the same length were prepared with varying proportion of FTSC-tagged polymer. Buffer hydration of these mixed films yielded fluorescent nanoparticle populations that showed no loss of fluorescence or detectable precipitation in serum at 37 °C. Cell uptake over a range of polymer concentration from 0.1 to 250 $\mu\text{g}/\text{mL}$ was studied in two widely used cell lines, A549 and MCF-7. Full retention by molecular weight cutoff filters greater than unimer size established that concentrations of 0.1 $\mu\text{g}/\text{mL}$ were safely above polymer critical micelle concentration (cmc) for all three block copolymer lengths; thus, conditions reflect nanoparticle uptake rather than uptake of soluble polymer. Following a 6 h incubation and wash, cells were trypsinized, fixed and analyzed by FACS or fixed and examined by epifluorescence microscopy. Interestingly, while both cell types showed increased fluorescence, there was significantly higher uptake by MCF-7 for reasons we do not understand (Figure 7). Though this polyacrylate architecture has been well-studied,²² this is the first report of its cell uptake profile, enabled by polymer end-labeling. Dose dependence of uptake was established for the MCF-7 cell line, with increased fluorescence correlating with higher degree of polymer labeling and total polymer concentration.

CONCLUSIONS

Using a ketone-modified Z-group on a trithiocarbonate RAFT agent, we have demonstrated effective and practical hydrazone conjugation of amphiphilic block copolymers of the general form PnB-*b*-PAA, using reporter tags commonly required for biotechnological applications such as imaging, bioconjugation, and targeting. Polymer–ketone conjugation with hydrazide

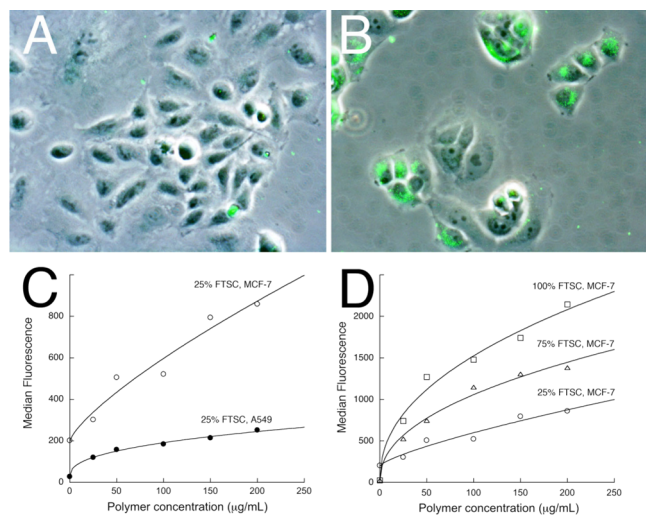


Figure 7. Cellular uptake studies on FTSC labeled $\mathbf{Pb}_{(100,89)}$. Overlaid phase contrast and fluorescein epifluorescence microscopy images of washed and fixed (A) A549 cells and (B) MCF-7 cells after incubation with nanoparticles composed of 25% FTSC-labeled $\mathbf{Pb}_{(100,89)}$ and 75% $\mathbf{Pe}_{(100,89)}$. Relative uptake profiles obtained by FACS are shown of (C) MCF-7 vs A549 cells and (D) fluorescence in MCF-7 cells, as proportion of labeled $\mathbf{Pb}_{(100,89)}$ is increased as indicated.

derivatives of FITC, biotin, and Gd-DOTA yielded the expected fluorescent, protein-binding, and relaxivity properties in the assembled polymer nanoparticle. This strategy, in combination with nanoparticle encapsulation strategies,²⁸ could conveniently generate nanoparticle assemblies with multiple functions. Discrete end-functionalization methodology also enables necessary assembly characterization: fluorophore installation allowed convenient determination of the upper limit of polymer cmc and tracking of cellular uptake of polymer nanoparticles without disruption of particle core packing interactions. Overall, hydrazone conjugation to the Z-group appears entirely stable to handling and extended incubation under physiological pH and temperature, despite the known lability of the trithiocarbonate linkage to nucleophilic attack. Therefore, this method of polymer end-functionalization

provides a synthetically convenient and useful complement to known methods of modification at the reinitiator "R" site of RAFT agents. Synthetic possibilities in polymer architecture may be broadened by a combination of the two approaches to CTA derivatization.

■ ASSOCIATED CONTENT

Supporting Information

Additional experimental details, compound characterization, TEM. This material is available free of charge via the Internet at <http://pubs.acs.org>.

■ AUTHOR INFORMATION

Corresponding Author

*E-mail: bong@chem.osu.edu.

Notes

The authors declare no competing financial interest.

■ ACKNOWLEDGMENTS

This work was supported in part by NSF-0927778, NSF-0747194 (D.B.), and NIH-HL106487 (S.R.).

■ REFERENCES

- (1) (a) Keddie, D. J.; Moad, G.; Rizzardo, E.; Thang, S. H. *Macromolecules* **2012**, *45*, 5321–5342. (b) Moad, G.; Rizzardo, E.; Thang, S. H. *Acc. Chem. Res.* **2008**, *41*, 1133–1142. (c) Boyer, C.; Stenzel, M. H.; Davis, T. P. *J. Polym. Sci., Part A: Polym. Chem.* **2011**, *49*, 551–595. (d) Stenzel, M. H. *Chem. Commun.* **2008**, *2008*, 3486–3503.
- (2) (a) Braunecker, W. A.; Matyjaszewski, K. *Prog. Polym. Sci.* **2007**, *32*, 93–146. (b) Zetterlund, P. B.; Kagawa, Y.; Okubo, M. *Chem. Rev.* **2008**, *108*, 3747–3794.
- (3) Boyer, C.; Bulmus, V.; Davis, T. P.; Ladmiral, V.; Liu, J.; Perrier, S. *Chem. Rev.* **2009**, *109*, 5402–5436.
- (4) (a) Maibaum, L.; Dinner, A. R.; Chandler, D. *J. Phys. Chem. B* **2004**, *108*, 6778–6781. (b) Discher, D. E.; Eisenberg, A. *Science* **2002**, *297*, 967–973.
- (5) Bartels, J. W.; Cauet, S. I.; Billings, P. L.; Lin, L. Y.; Zhu, J.; Fidge, C.; Pochan, D. J.; Wooley, K. L. *Macromolecules* **2010**, *43*, 7128–7138.
- (6) Immordino, M. L.; Dosio, F.; Cattel, L. *Int. J. Nanomed.* **2006**, *1*, 297–315.
- (7) (a) Knop, K.; Hoogenboom, R.; Fischer, D.; Schubert, U. S. *Angew. Chem., Int. Ed.* **2010**, *49*, 6288–6308. (b) Kang, J. S.; Deluca, P. P.; Lee, K. C. *Expert Opin. Emerging Drugs* **2009**, *14*, 363–380. (c) Veronese, F. M.; Mero, A.; Pasut, G. *PEGylated Protein Drugs* **2009**, *11*–31. (d) Fishburn, C. S. *J. Pharm. Sci.* **2008**, *97*, 4167–4183.
- (8) (a) Elsabahy, M.; Wooley, K. L. *Chem. Soc. Rev.* **2012**, *41*, 2545–2561. (b) Geng, Y.; Dalhaimer, P.; Cai, S.; Tsai, R.; Tewari, M.; Minko, T.; Discher, D. E. *Nat. Nanotechnol.* **2007**, *2*, 249–255.
- (9) Bathfield, M. I.; D'Agosto, F.; Spitz, R.; Charreyre, M.-T. r. s.; Delair, T. *J. Am. Chem. Soc.* **2006**, *128*, 2546–2547.
- (10) Bontempo, D.; Maynard, H. D. *J. Am. Chem. Soc.* **2005**, *127*, 6508–6509.
- (11) (a) Moad, G.; Rizzardo, E.; Thang, S. H. *Polym. Int.* **2011**, *60*, 9–25. (b) Tasdelen, M. A.; Kahveci, M. U.; Yagci, Y. *Prog. Polym. Sci.* **2011**, *36*, 455–567.
- (12) York, A. W.; Kirkland, S. E.; McCormick, C. L. *Adv. Drug Delivery Rev.* **2008**, *60*, 1018–1036.
- (13) (a) Kalia, J.; Raines, R. T. *Angew. Chem., Int. Ed.* **2008**, *47*, 7523–7526. (b) Kalia, J.; Raines, R. T. *Curr. Org. Chem.* **2010**, *14*, 138–147.
- (14) (a) Frullano, L.; Tejerina, B.; Meade, T. J. *Inorg. Chem.* **2006**, *45*, 8489–8491. (b) Lee, C. C.; Gillies, E. R.; Fox, M. E.; Guillaudeu, S. J.; Frechet, J. M.; Dy, E. E.; Szoka, F. C. *Proc. Natl. Acad. Sci. U. S. A.* **2006**, *103*, 16649–16654. (c) Kale, A. A.; Torchilin, V. P. *Bioconjugate Chem.* **2007**, *18*, 363–370.
- (15) Li, Y.; Lokitz, B. S.; McCormick, C. L. *Macromolecules* **2005**, *39*, 81–89.
- (16) (a) Vázquez-Dorbatt, V.; Tolstyka, Z. P.; Maynard, H. D. *Macromolecules* **2009**, *42*, 7650–7656. (b) Grover, G. N.; Lee, J.; Matsumoto, N. M.; Maynard, H. D. *Macromolecules* **2012**, *45*, 4958–4965.
- (17) Jackson, A. W.; Fulton, D. A. *Macromolecules* **2009**, *43*, 1069–1075.
- (18) Lai, J. T.; Filla, D.; Shea, R. *Macromolecules* **2002**, *35*, 6754–6756.
- (19) Nakamura, Y.; Kitada, Y.; Kobayashi, Y.; Ray, B.; Yamago, S. *Macromolecules* **2011**, *44*, 8388–8397.
- (20) Coster, M. J.; De Voss, J. J. *Org. Lett.* **2002**, *4*, 3047–3050.
- (21) Kim, J. Y.; Chae, H. K.; Choi, B. C.; Ha, H.-J.; Oh, S. J. *Bull. Korean Chem. Soc.* **2004**, *35*, 1512–1514.
- (22) (a) Lejeune, E.; Chassenieux, C.; Colombani, O. *Prog. Colloid Polym. Sci.* **2011**, *138*, 7–16. (b) Lejeune, E.; Drechsler, M.; Jestin, J.; Müller, A. H. E.; Chassenieux, C.; Colombani, O. *Macromolecules* **2010**, *43*, 2667–2671. (c) Nicolai, T.; Colombani, O.; Chassenieux, C. *Soft Matter* **2010**, *6*, 3111–3118.
- (23) Thomas, D. B.; Convertine, A. J.; Hester, R. D.; Lowe, A. B.; McCormick, C. L. *Macromolecules* **2004**, *37*, 1735–1741.
- (24) (a) Litvinenko, G.; Müller, A. H. E. *Macromolecules* **1997**, *30*, 1253–1266. (b) Müller, A. H. E.; Zhuang, R.; Yan, D.; Litvinenko, G. *Macromolecules* **1995**, *28*, 4326–4333. (c) Chong, Y. K.; Krstina, J.; Le, T. P. T.; Moad, G.; Postma, A.; Rizzardo, E.; Thang, S. H. *Macromolecules* **2003**, *36*, 2256–2272.
- (25) Smith-Palmer, T.; Barbarakis, M. S.; Cynkowski, T.; Bachas, L. G. *Anal. Chim. Acta* **1993**, *279*, 287–292.
- (26) Qi, K.; Ma, Q.; Remsen, E. E.; Clark; Wooley, K. L. *J. Am. Chem. Soc.* **2004**, *126*, 6599–6607.
- (27) (a) Perrault, S. D.; Walkey, C.; Jennings, T.; Fischer, H. C.; Chan, W. C. W. *Nano Lett.* **2009**, *9*, 1909–1915. (b) Jain, R. K.; Stylianopoulos, T. *Nat. Rev. Clin. Oncol.* **2010**, *7*, 653–664. (c) Phillips, M. A.; Gran, M. L.; Peppas, N. A. *Nano Today* **2010**, *5*, 143–159.
- (28) (a) Horacio, C.; Kazunori, K. *Sci. Technol. Adv. Mater.* **2010**, *11*, 014109. (b) Janib, S. M.; Moses, A. S.; MacKay, J. A. *Adv. Drug Delivery Rev.* **2010**, *62*, 1052–1063.
- (29) Lee, S. M.; Song, Y.; Hong, B. J.; MacRenaris, K. W.; Mastarone, D. J.; O'Halloran, T. V.; Meade, T. J.; Nguyen, S. T. *Angew. Chem., Int. Ed.* **2010**, *49*, 9960–9964.
- (30) Briley-Saebo, K. C.; Geninatti-Crich, S.; Cormode, D. P.; Barazza, A.; Mulder, W. J. M.; Chen, W.; Giovenzana, G. B.; Fisher, E. A.; Aime, S.; Fayad, Z. A. *J. Phys. Chem. B* **2009**, *113*, 6283–6289.